scientific reports

Check for updates

OPEN

Association between blink-related anterior segment dynamics and intraocular pressure

Vito Ivano D'Alessandro[1,2], Filippo Attivissimo[1], Attilio Di Nisio[1], Anna Lanzolla[1], Amal Isaiah[3,4] & Giuliano Scarcelli[2]✉

Intraocular pressure (IOP) is a key parameter for diagnosing and managing glaucoma. This study introduces a novel, non-contact method for evaluating blink-induced anterior segment dynamics, as observed through corneal profile motion during natural blinking, demonstrating its dependence on IOP. The eyelid deforms the corneal surface during a blink, resulting in a rebound response. A high-speed lateral imaging system tracked corneal profile motion in healthy volunteers during the eye-opening phase. Changes in anterior segment dynamics were analyzed at baseline and after the Valsalva maneuver to increase IOP. Two metrics were measured in both conditions: the time constant τ, linked to the rebound speed, and the displacement amplitude A, measuring the extent of longitudinal corneal profile displacement. Fifteen participants without ocular disease were enrolled. The longitudinal displacement of the corneal profile revealed faster anterior segment dynamics during the Valsalva maneuver compared to the baseline. We identified a statistically significant difference in τ related to the rebound velocity between the baseline and Valsalva conditions ($P < 0.05$) but not for A. The proposed non-contact technique demonstrates sensitivity to IOP variations by analyzing anterior segment dynamics during a natural, complete blink, which supports further assessment of potential home-based, frequent IOP monitoring to prevent glaucoma progression and vision loss.

Keywords Anterior segment dynamics, Eye blinking, Eye retraction, Glaucoma, Image segmentation, Intraocular pressure (IOP)

Intraocular pressure (IOP) is the sole modifiable risk factor for glaucoma, the leading cause of irreversible blindness worldwide, affecting approximately 3.5% of the global population aged 40–80 years[1,2]. Therefore, accurate assessment and monitoring of IOP are crucial for early diagnosis and management of this ocular disease. This study investigates the potential of blinking, a natural physiological process that serves various functions, including lubrication of the ocular surface, debris removal, and eye protection[3,4], to determine blink-induced anterior segment dynamics, as observed through corneal profile motion tracking, and explore its potential dependence on IOP.

IOP is typically measured by tonometry, with the Goldmann Applanation Tonometer (GAT) as the gold standard[5]. GAT requires contact with the eye in a clinical setting and requires topical anesthetics and professional expertise. Moreover, GAT can neither be used at home, nor for continuous monitoring that could help detect glaucoma early. To address these issues, various innovations have been introduced. For example, smart contact lenses embedded with sensors provide continuous IOP monitoring, yet require corneal contact and may not be acceptable by all[6–8]. Implantable sensors[9,10] provide direct measurements but require invasive surgery[11]. Here we propose a novel non-contact method to evaluate anterior segment dynamics associated with natural blinking and assess its correlation with IOP. This method leverages the natural eyelid pressure (ELP) exerted on the corneal surface[12,13] during a blink to analyze IOP-related corneal deformation. While the individual contributions of corneal deformation and eye globe translation cannot be decoupled with the current setup, their combined response during a natural blink provides access to IOP-dependent anterior segment biomechanical information, potentially supporting the development of non-contact, home-based strategies for continuous IOP monitoring.

[1]Department of Electric and Information Engineering, Polytechnic University of Bari, Bari, Italy. [2]Fischell Department of Bioengineering, University of Maryland, College Park, MD, USA. [3]Department of Otorhinolaryngology–Head and Neck Surgery, University of Maryland School of Medicine, Baltimore, MD, USA. [4]University of Maryland Institute for Health Computing, Bethesda, MD, USA. ✉email: scarc@umd.edu

Materials and methods

Imaging system

The imaging system developed to track the corneal profile motion to assess the anterior segment dynamics during eye blinking is depicted in Fig. 1a. The setup comprises a modified ophthalmology slit lamp and an imaging lens (focal length of 50 mm, numerical aperture of 0.18; Thorlabs, Newton, NJ). This system is integrated with a high-frame-rate (510 FPS) camera (Allied Vision, Edmund Optics, Barrington, NJ) placed lateral to the participant's eye to capture the corneal profile during each blink. The videos were acquired in 8-bit grayscale format with a spatial resolution of 800×600 pixels. Since the camera operates at 510 FPS, resulting in a low exposure time, a visible LED ring light aligned concentrically with the camera lens was employed as the illumination source, allowing a broader dynamic range [0–255] of grayscale values for improved image quality[14,15]. An example lateral eye image is shown in Fig. 1b.

Participants and experimental protocol

We included healthy volunteers aged 18–50 without history of ocular or systemic conditions that could influence IOP. All participants provided written informed consent. The study was conducted in compliance with the Declaration of Helsinki and approved by the Institutional Review Board (IRB) of the University of Maryland Baltimore. Each participant was assessed under two experimental conditions to examine anterior segment dynamics during a natural, complete blink (baseline) and during a Valsalva maneuver. For each participant, data were acquired only from the left eye.

The experimental protocol consisted of four steps. First, baseline IOP was measured using a portable tonometer (iCare IC200, Icare USA, Inc., Raleigh, NC, USA)[16], an FDA-approved medical device comparable to the Goldmann Applanation Tonometer (GAT)[17,18].

Next, participants were asked to blink naturally while their eye movements were recorded using the high-speed imaging system. To ensure consistency in imaging geometry, each participant positioned their head on a modified chin rest, which prevented head tilt and maintained a constant imaging angle relative to the camera.

Then, participants were instructed to perform the Valsalva maneuver, which is known to raise IOP[19–21]. This technique required them to exhale forcefully against a closed glottis into an air tube connected to an analog manometer, maintaining a pressure of at least 40 mmHg for 15 s[22].

The elevation of IOP during the Valsalva maneuver was confirmed with the portable tonometer. The maneuver was successful only if the IOP increased by more than 1 mmHg. If participants failed to maintain the required pressure or the IOP increase did not meet this threshold, they were asked to repeat the experiment. Finally, additional blinks and associated dynamics were recorded while participants performed the Valsalva maneuver. Participants were excluded if their eyelashes obstructed the corneal profile, preventing reliable measurement of anterior segment dynamics.

Data acquisition and analysis

A software program (StreamPix, NorPix Inc., Montreal, CA) was used to record blinks under two conditions: baseline and Valsalva. For the baseline condition, single or multiple videos totaling one minute in duration were recorded, during which participants were asked to perform natural blinks. For the Valsalva condition, multiple

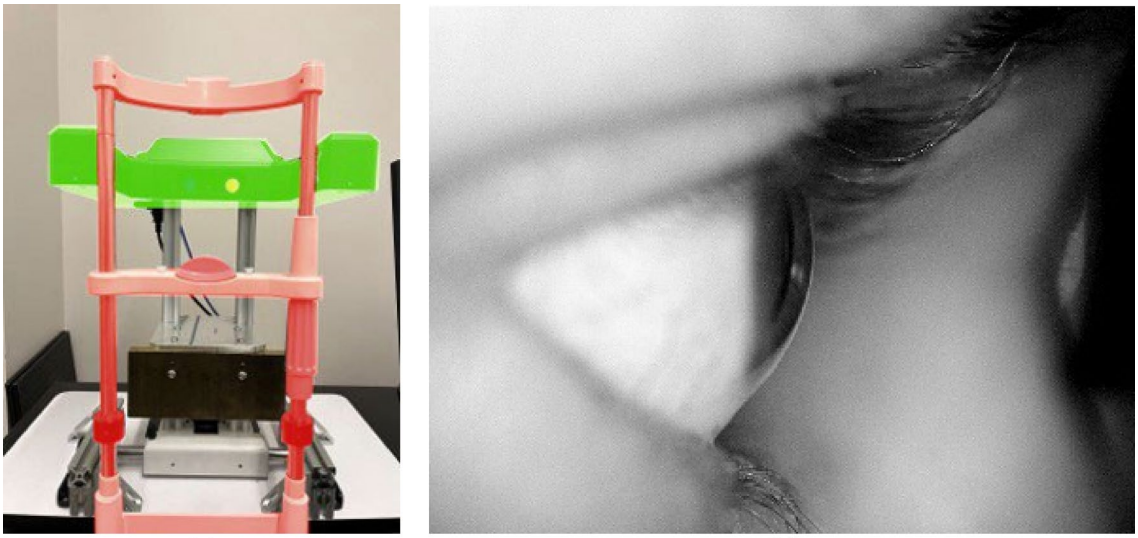

(a) **(b)**

Fig. 1. High-speed imaging system to track corneal profiles during a blink. (**a**) Side and front views of the imaging system. The green area represents the chassis housing the cameras and lenses, and the red structure is the modified chin rest where the patient rests his head for image acquisition. (**b**) An example of the lateral eye image acquired with the imaging system.

videos were recorded as each maneuver lasted approximately 15 s. A minimum of five blinks was considered acceptable for each condition.

Using a built-in MATLAB application (Video Viewer; MathWorks Inc., Natick, MA, USA), the blinks in the recorded videos were manually identified, determining the start and end frames of the eye-opening phase, from a fully closed eye to a fully open eye. During this manual eye blinking detection process, certain blinks were discarded based on the following criteria: (i) multiple blinks, when two or more consecutive blinks occur in rapid succession, making it difficult to isolate a single eye-opening phase. These were identified by the absence of a stable, fully open eye state between two consecutive closures. (ii) incomplete blinks, when the eye does not fully close before reopening, and (iii) excessive facial muscle activation, when significant movement of the eyebrows, forehead, or cheeks was observed, suggesting facial contractions that could interfere with the natural anterior segment response. Only natural and complete blinks were further analyzed.

A custom Python script was used to train a neural network specifically designed to predict eye masks during the eye-opening phase of each blink. The predicted ocular masks were subsequently used to quantify blink-related anterior segment dynamics, as inferred from corneal profile motion tracking during each blink. An exponential-like curve was produced for all the blinks by evaluating the longitudinal corneal displacement over time. The following parameters were computed: (i) the time constant, which quantifies the rebound velocity of the anterior segment during a natural, complete blink, and (ii) the displacement amplitude, which represents the extent of translation of the corneal profile (Fig. 3e).

Neural network training

For each participant, at least two eye-blinking frames were manually labeled, one from the baseline and one from elevated IOP conditions, resulting in approximately 400 labeled images per participant. These manually labeled images were then used to train a modified U-Net[23] neural network for segmenting the ocular region. The network was initialized and trained individually for each participant, using only their respective eye images, ensuring that the model was optimized for each participant. The architecture consisted of convolutional layers with filters ranging from 64 to 512, with a bottleneck containing 1024 filters. Batch normalization layers were included after each convolution to improve the convergence rate and stability of the training process. The input images were resized to [256, 256] pixels and normalized in the range [0, 1] before being fed into the neural network.

Frames related to the opening phase of blinking were classified into four different classes: closed eye, semi-closed eye, semi-open eye, and open eye. A resampling method based on the mask area was applied to address the potential class imbalance. Masks were categorized as follows: (i) closed eye: masks with zero area, (ii) semi-closed eye: masks with an area between 0% and 40% of the maximum observed area. (iii) semi-open eye: masks with an area between 40% and 80% of the maximum observed area, (iv) open eye: masks with an area greater than 80% of the maximum observed area. An example of the classification of these images based on the mask area is shown in Fig. 2.

After classification, a random resampling approach was employed to increase the number of images in underrepresented classes. Specifically, we resampled images and masks to match the number of samples in the majority class, ensuring a balanced distribution. In addition to resampling, data augmentation techniques were applied to enhance the diversity of the training dataset[24]. The following transformations were used to facilitate

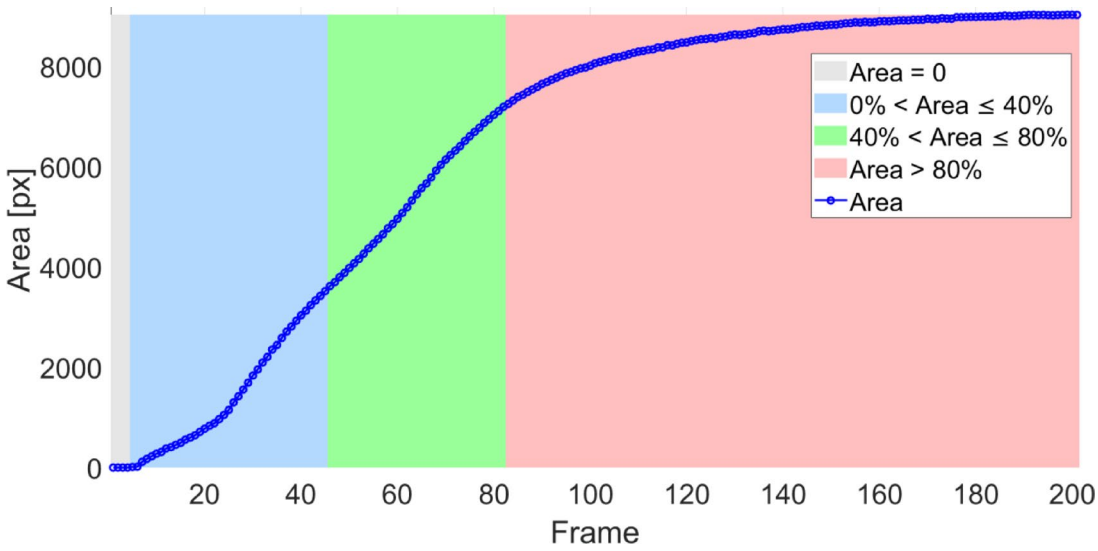

Fig. 2. Example of the classification method based on the mask area. The curve represents the segmented area over the sequence of frames during the eye-opening blink phase. Each frame is classified into four categories: closed eye (gray, area = 0), semi-closed eye (blue, area between 0% and 40% of the maximum), semi-open eye (green, area between 40% and 80% of the maximum), and open eye (red, area > 80% of the maximum). This classification was used to balance the dataset for neural network training.

model generalization for various eye positions: (i) flip: images were horizontally flipped. (ii) rotation: images were randomly rotated within a range of ± 10 degrees to account for slight variations in head pose. (iii) zoom: images were randomly scaled up or down within ± 10% of their dimensions, and (iv) translation: images were randomly translated up to ± 10% of the frame dimensions in both vertical and horizontal directions to simulate slight head movements.

The dataset was subsequently split into 80% for training and 20% for validation. The neural network was trained with a batch size of 16, the Adam optimizer, an initial learning rate of $1e^{-3}$ and a maximum of 200 epochs. Early stopping based on validation loss and a reduced learning rate on plateau strategy were implemented during training to prevent overfitting and enhance generalization. The loss function used for training is the combo loss, a weighted sum of Binary Crossentropy (BCE) and Dice Loss. The BCE component effectively penalizes incorrect predictions for each pixel, handling output imbalance[25]; on the other hand, the Dice Loss is particularly effective in addressing input imbalance[26], as it emphasizes the overlap between predicted and ground truth masks. This combination leverages the strengths of both loss functions, improving the network's ability to learn from imbalanced data while maintaining segmentation accuracy[27]. This approach is particularly suitable for our application since semi-closed eye frames are heavily imbalanced in terms of foreground and background pixels.

The performance of the trained model was evaluated using the Intersection over Union (IoU) metric, which measures the overlap between the predicted and ground-truth masks.

For each participant, the trained model achieved an IoU score greater than 90% on the test dataset. Then, the trained network predicted eye masks for all other blinks of the same participant, significantly accelerating the manual labeling process. Figure 3a-d shows the predicted masks generated by the neural network for four distinct frames of a participant's blink overlaid on the original images, showing the progression from a slight to a fully open eye.

Corneal profile extraction

After predicting ocular masks using the trained network, the corneal profile for each frame was extracted through a series of processing steps. First, the centroid of the predicted mask was determined, representing the geometric center of its pixel distribution. Masks without a valid centroid, such as empty masks or those containing multiple disconnected regions, were excluded from further analysis.

First, the mask was skeletonized to isolate the corneal profile. Pixels located to the right of the centroid were then analyzed to identify two key points: the upper-right pixel and the lower-right pixel. The upper-right pixel was determined as the farthest pixel above the centroid along the y-axis, selected based on the Euclidean distance from the centroid. Similarly, the lower-right pixel was identified as the pixel with the minimum y-coordinate below the centroid. In cases where multiple pixels shared the same y-coordinate, the pixel with the highest x-coordinate was chosen. With the upper-right and lower-right points established, a geodesic distance algorithm was applied to the skeletonized ocular mask to compute the shortest path between these two key points. This shortest path is consistently aligned with the corneal profile for every frame, spanning from the frame where the eye is slightly open to the frame where it is fully open.

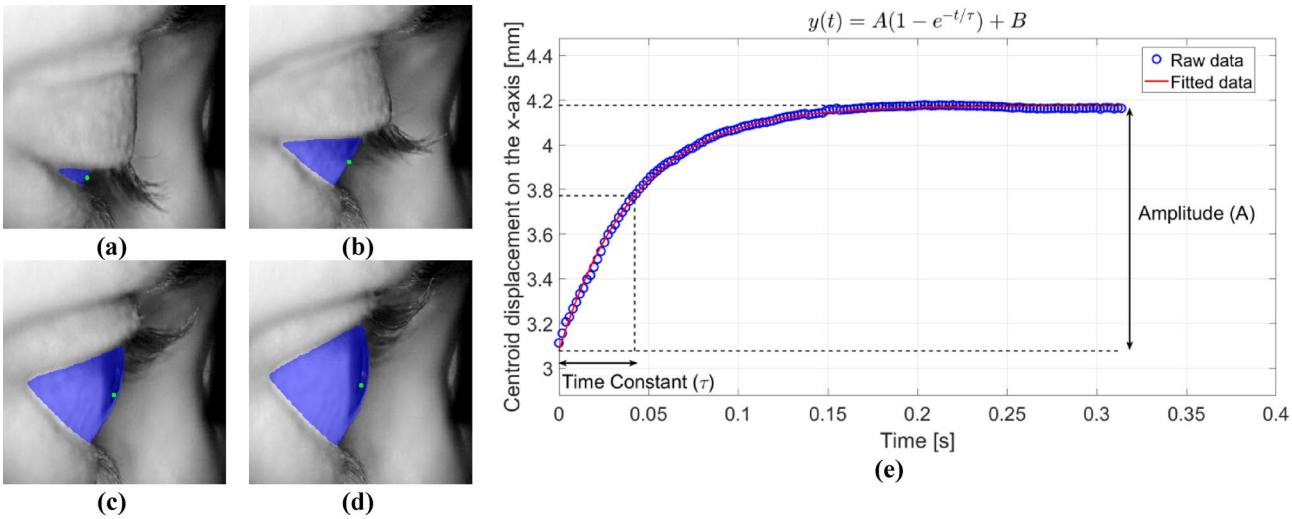

Fig. 3. Evaluation of corneal profile motion during a blink. (**a-d**) Sequential frames from a blink show the transition from a slightly open-eye state to a fully open-eye state, with the predicted corneal masks from the neural network overlaid in blue. The green dot indicates the centroid of the corneal profile. (**e**) Corneal centroid displacement along the x-axis during the eye-opening phase, including raw data (blue circles) and the corresponding exponential fit (red line) based on the two key metrics (τ and A).

Anterior segment dynamics analysis

Anterior segment dynamics was assessed by tracking the corneal profile motion during the eye-opening phase of a natural, complete blink. Indeed, the longitudinal displacement of the corneal profile during a blink was measured. More in-depth, we examined its centroid (which is different from the eye mask's centroid), based on the pixel distribution along the corneal profile. The displacement of the centroid followed an exponential trajectory, reaching a plateau when the eye is fully open. Therefore, we modeled raw data using an exponential fitting function, defined as:

$$y(t) = A\left(1 - e^{\frac{-t}{\tau}}\right) + B \tag{1}$$

where A represents the displacement amplitude, which reveals the extent of movement of the corneal profile; B is the offset and τ is the time constant, which quantifies the rebound velocity of the corneal profile during the eye-opening phase of the blink after being deformed by the force applied by the eyelids.

It is important to note that the corneal profile motion analyzed in this study reflects a superposition of corneal deformation induced by eyelid pressure and eye retraction occurring during blinking. As these two contributions cannot be independently separated with the current system, the measured corneal profile dynamics should be interpreted as representative of the combined mechanical response of the anterior segment. Consequently, the extracted parameters describe blink-related anterior segment dynamics rather than isolated corneal deformation.

Since the imaging angle was fixed by the modified chin rest during acquisition, variations among participants were limited to small differences in the relative position of the eye within the camera's field of view (e.g., slightly higher or lower, or shifted left or right eye position). Such variations affect only the offset parameter (B) of the exponential fitting, which corresponds to the initial position of the corneal profile centroid, but likely do not influence the dynamic parameters (τ and A) that describe the anterior segment dynamics. An example of the exponential fitting, and its parameters, applied to the raw data of longitudinal corneal displacement is depicted in Fig. 3e.

Before applying exponential fitting, potential outliers in the centroid displacement data were removed. Specifically, the first five frames of each blink's opening phase were excluded, as these frames often present challenges for the neural network in accurately predicting the eye's mask due to partial obstruction of the corneal profile by eyelashes.

A filtering step was applied to the fitted curves based on their fitted parameters as the root mean square error (RMSE) and R^2. Specifically, R^2 values below $\mu_{R^2} - 3\sigma_{R^2}$ and RMSE values exceeding $\mu_{RMSE} + 3\sigma_{RMSE}$ were considered outliers.

This filtering process allows us to exclude blinks with poorly fitted curves, resulting from segmentation errors, non-natural blinks, or head movements during the blink acquisition process. To evaluate differences in the anterior segment dynamics under baseline and during the Valsalva maneuver, the two parameters of the fitted curves, τ and A, were analyzed.

A second filtering process was applied to the curves to obtain the most accurate estimate of τ for each condition and participant. Specifically, only curves with a z-score within 1 were included for the baseline and Valsalva IOP conditions.

To validate this approach, ten consecutive one-minute videos were acquired from a single participant under baseline IOP conditions. From these recordings, 206 complete and natural blinks met the inclusion criteria and were analyzed to assess the normality. The Kolmogorov–Smirnov test confirmed that τ followed a normal distribution ($P = 0.115$), supporting the statistical assumptions needed to apply this filtering method. In addition, this analysis allowed us to evaluate the repeatability of the proposed method under identical baseline conditions. The parameters showed low intra-subject variability, with mean ± SD values of $\tau = 50.9 \pm 7.6\, ms$ and $A = 1.16 \pm 0.08\, mm$, corresponding to coefficients of variation of 15% and 7%, respectively. These results demonstrate that the method provides reliable and repeatable measurements of anterior segment dynamics during blinking, enabling the detection of IOP-related variations.

Finally, the average τ and amplitude were calculated for the remaining baseline and Valsalva IOP trajectories after this filtering process.

Under elevated IOP conditions, induced by the Valsalva maneuver, we hypothesize that the anterior segment rebounds faster due to the higher internal pressure exerting an increased restoring force. Consequently, a lower τ is expected for the Valsalva condition, reflecting faster anterior segment dynamics than the baseline IOP condition.

Results

Fifteen healthy participants (28.3 ± 6.02 years; 10 males, 5 females) were enrolled in the study and included in the final analysis. Each participant successfully performed the Valsalva maneuver, which was well tolerated without any adverse events during or after the procedure.

Anterior segment dynamics for a single sample

Initially, nine blinks were recorded under baseline IOP conditions and ten under elevated IOP (Valsalva) conditions. After applying the filtering process, six blinks from each condition were selected for further analysis. Figure 4a shows the corneal centroid displacement along the x-axis during the blink's opening phase for a single participant. In both conditions, the trajectory of the corneal centroid exhibits an exponential trend, stabilizing as the eye reaches its fully open state.

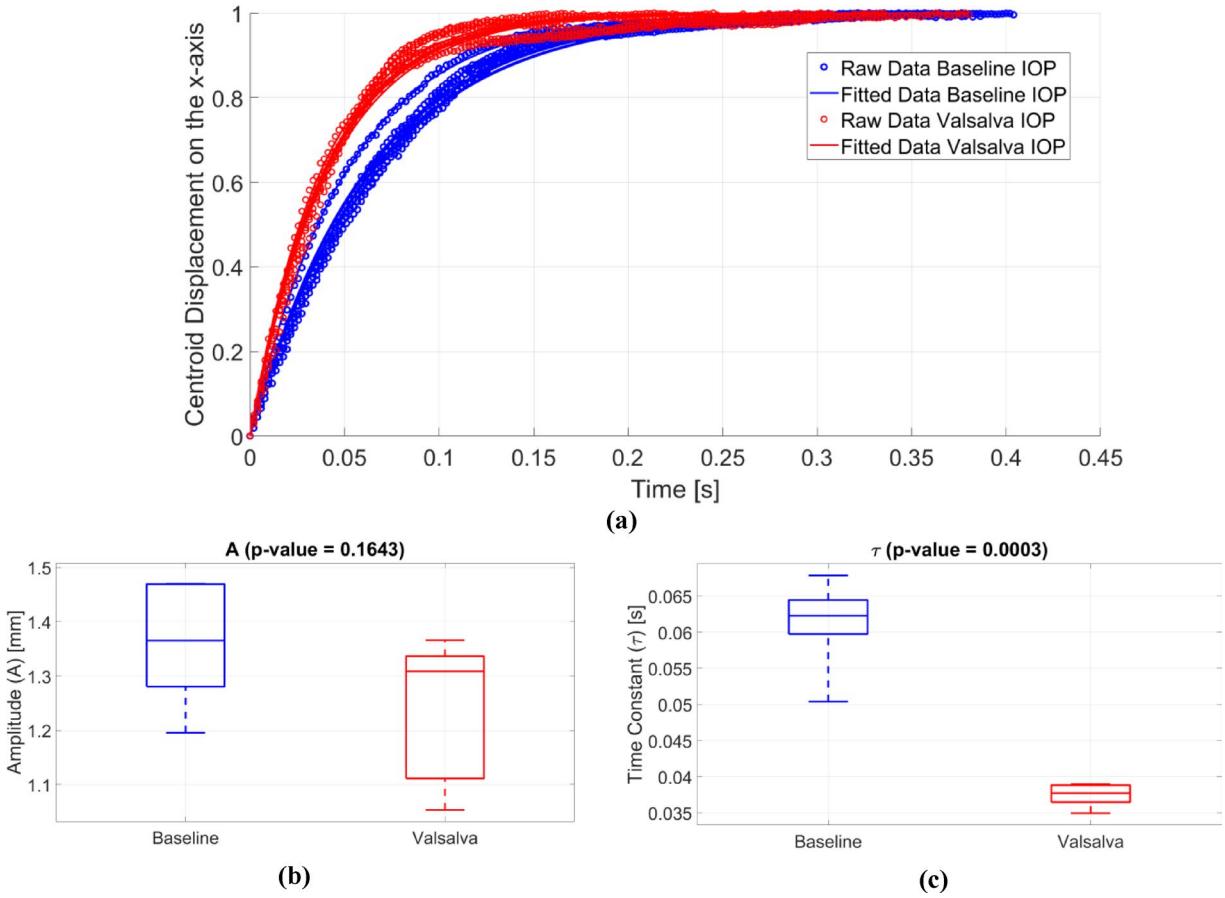

Fig. 4. Blink-related anterior segment dynamics for a single participant in baseline and elevated IOP conditions. (**a**) Normalized longitudinal centroid displacement during the blinks' opening phase. The blue curves represent the displacement under baseline IOP condition, whereas the red curves correspond to the displacement under elevated IOP condition (Valsalva). Normalization was applied only for visualization, as eye positions may vary across blinks recorded in different videos. (**b**) A of baseline versus elevated IOP conditions. (**c**) τ of baseline versus elevated IOP conditions.

The parameters τ and A were measured from the corneal profile motion during the blink's opening phase for both conditions. The results showed that τ was lower in the Valsalva condition (37.44 ± 0.64 ms) compared to the baseline (61.17 ± 2.44 ms), and this difference was statistically significant ($t = 9.42$, $P < 0.001$, Fig. 4c).

Regarding A, the average for the baseline IOP condition was $1.36 \pm 0.04\, mm$, and for the Valsalva condition, it was $1.25 \pm 0.05\, mm$, and this difference was not statistically significant (Fig. 4b).

Statistical analysis

To assess the effectiveness of the Valsalva maneuver in increasing IOP, we compared IOP values measured before and after the maneuver across all participants using the portable tonometer. The mean baseline IOP was $18.55 \pm 0.72\, mmHg$, while the mean IOP during the Valsalva condition increased to $23.73 \pm 1.01\, mmHg$. This increase was statistically significant ($t = 6.78$, $P < 0.001$), confirming that the Valsalva maneuver induced a consistent and measurable elevation in IOP, with IOP difference ranging from $1.7\, mmHg$ to $13\, mmHg$ between the two conditions.

To determine whether the IOP-dependent behavior observed in a single subject was consistent among participants, we performed a statistical analysis on all enrolled samples. Parameters τ and A were compared between baseline and elevated IOP conditions using a paired t-test.

Figure 5a illustrates the variation of τ for each participant who underwent the experiment. Out of 15 samples, 11 exhibit the expected trend, showing a lower τ under the elevated IOP condition compared to the baseline IOP condition.

The average τ was $46.23 \pm 2.48\, ms$ for the baseline IOP condition and $39.73 \pm 1.31\, ms$ for the elevated IOP condition ($t = -2.56$, $P < 0.05$, Fig. 5a), which indicates a faster anterior segment rebound when the Valsalva maneuver is performed. Figure 5b depicts the changes in A for each participant across the two IOP conditions, with the color scale indicating the change in the amplitude ΔA between baseline and elevated IOP conditions. The average amplitude was $1.05 \pm 0.08\, mm\, px$ for the baseline IOP and $1.04 \pm 0.08\, mm$ for

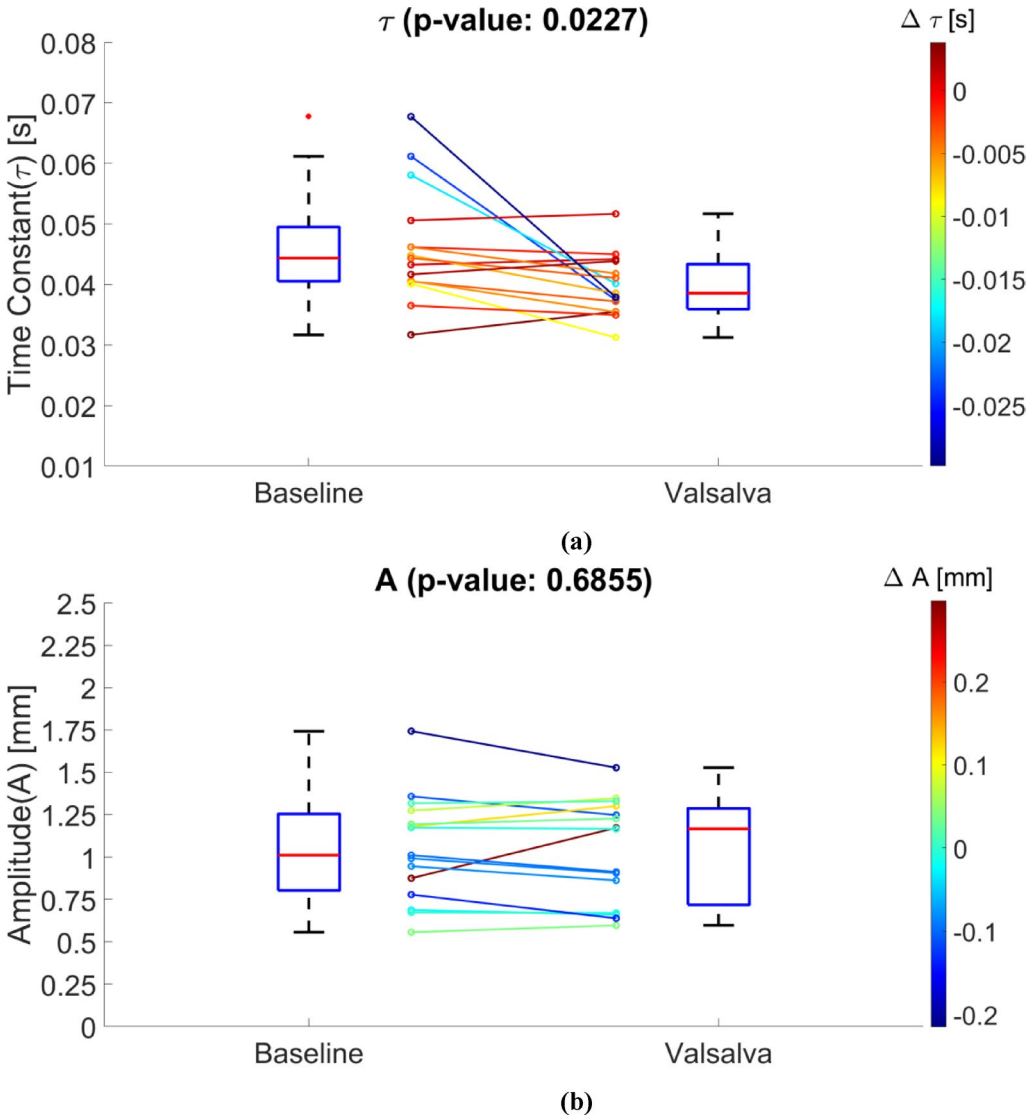

Fig. 5. Statistical analysis for 15 healthy samples without ocular disease history. (**a**) τ of normal and Valsalva IOP conditions across 15 samples ($P < 0.05$). (**b**) A of baseline and Valsalva IOP conditions across 15 samples (no statistically significant difference).

the elevated IOP condition. Unlike τ , A does not exhibit a clear or consistent pattern across participants, with changes appearing more variable and without a statistically significant difference.

Furthermore, to confirm the results obtained from the paired t-test, the Wilcoxon signed-rank test was applied, as it is more robust to outliers, does not assume normality of the data and is suitable for a small sample size. The test confirmed the statistical difference observed for τ ($P = 0.0125$), supporting the evidence of a faster anterior segment rebound under elevated IOP conditions. Conversely, the comparison of A between baseline and Valsalva conditions remained not statistically significant ($P = 0.495$), consistent with the paired t-test results.

In addition, we investigated whether the blink-derived biomechanical parameters were associated with baseline IOP. Spearman's rank correlation coefficients were computed between baseline IOP and the parameters τ and A. No significant correlation was found between τ and baseline IOP ($\rho = -0.25$, $P = 0.38$) or between A and baseline IOP ($\rho = -0.17$, $P = 0.54$). Although these associations were not statistically significant, both parameters exhibited a weak negative trend, also demonstrating a tendency toward faster anterior segment rebound (lower τ) at higher IOP levels. In this context, the absence of a significant correlation between A and IOP is consistent with a previous report showing a weak and non-significant relationship between independently measured eye retraction amplitude and IOP[28].

Discussion

This study presents a novel imaging system that provides information on blink-related anterior segment dynamics, as observed through corneal profile motion tracking, during a natural, complete blink and its correlation with

IOP changes. Thus, anterior segment dynamics were analyzed under two conditions: baseline IOP and elevated IOP, obtained during the Valsalva maneuver.

The deformation of the cornea by the eyelid during a blink[29–32] provides an opportunity to assess IOP-dependence of this phenomenon. However, the corneal deformation depends on its topography and biomechanics, leading to observable changes in corneal dynamics[33–36]. As a result, various structural and pathological conditions may be potential modifiers of the observed corneal response. For instance, keratoconus leads to localized thinning and steepening of the cornea, altering its curvature and mechanical stiffness[37], which can modify the corneal response to ELP. Moreover, post-surgical eyes typically exhibit a lower corneal hysteresis, which reflects the viscoelastic damping response of the corneal tissue to the applied force and corneal resistance factor, which is related to the time-independent corneal response to the applied force[38]. These biomechanical changes can result in a slower rebound of the corneal profile and an altered displacement amplitude induced by ELP.

Lin et al.[39] further confirmed that ELP causes a flattening effect on the cornea, with biomechanical IOP correlating with eyelid pressure and corneal deformation during a blink. In the present study, the anterior segment dynamics during blinking does not reflect only the corneal deformation induced by ELP, as the observed corneal profile motion also includes a contribution from the eye retraction. Despite their combined contribution, we observed that the anterior segment dynamics is sensitive to IOP changes: the statistically significant decrease of τ under elevated IOP conditions indicates a faster rebound following eyelid-induced deformation. This behavior is consistent with the anterior segment acting as a pressurized, fluid-filled system, in which increased internal pressure generates a greater restoring force, leading to faster mechanical recovery. On the other hand, A did not significantly differ between conditions, indicating that the extent of corneal profile motion is consistent across the two conditions. The absence of a statistically significant difference in the amplitude suggests that the faster rebound under Valsalva conditions cannot be attributed to an increase in the magnitude of eye movement. Indeed, elevated IOP predominantly influences the anterior segment rebound velocity without affecting the displacement amplitude. The current prototype does not provide absolute IOP values. Instead, it extracts two biomechanical parameters, τ and A, that are sensitive to IOP variations. These parameters reflect the viscoelastic behavior of the cornea under physiological eyelid pressure and should be interpreted as IOP-dependent biomechanical indicators rather than direct tonometric measurements. This interpretation is supported by the analysis of the relationship between these parameters and the absolute IOP values: when assessing the correlation between baseline IOP and τ or A across participants, no statistically significant relationship was found for either parameter.

Compared to conventional tonometry or recent innovations (e.g. contact lenses, implantable sensors), which require contact with the eye or surgical implants and can only be performed during office visits with professional assistance, our technology, once miniaturized into a wearable device, can potentially provide continuous non-contact monitoring of IOP-dependent indicators without requiring significant patient expertise. A more accessible, user-friendly and frequent monitoring solution like this can lead to a better understanding of IOP patterns and their relationship to glaucoma progression. For instance, a study of IOP monitoring conducted outside of regular office hours found that peak 24-hour IOP was greater than the peak IOP observed during prior office visits in 62% of the patients. Notably, the results of 24-hour IOP monitoring led to an immediate treatment change in 36% of patients[40]. Therefore, this technology could facilitate the early detection of abnormal IOP fluctuations, enable more precise patient-based treatment strategies, and mitigate the impact of untreated glaucoma.

Several types of glaucoma exist, the most common being primary open-angle glaucoma which is characterized by elevated IOP values beyond the normal range and progressive optic nerve damage[41]. However, not all forms of glaucoma are associated with increased IOP[42]. In normal-tension glaucoma, IOP values remain within the clinically normal range, yet progressive optic nerve damage can still occur[43]. In such cases, analyzing IOP fluctuations throughout the day could be beneficial for the early detection of the disease[44], as patients with normal-tension glaucoma often exhibit greater diurnal IOP variability[45,46], even if additional IOP-independent factors have gained increasing relevance in detecting this ocular disease[47]. The proposed method can potentially assess these variations through frequent, non-invasive, home-based measurements. Conversely, ocular hypertension is characterized by IOP levels above the normal threshold despite the absence of optic nerve damage[48]. For these patients, the absolute IOP value remains the primary diagnostic metric.

To extend the proposed approach from indirectly detecting IOP variations to providing quantitative IOP values, a calibration phase would be required. This phase would involve acquiring data from a cohort of patients showing controlled IOP changes and correlating the variations in biomechanical parameters with the corresponding changes in IOP measured by standard tonometry. Once this relationship is established, a single reference tonometric measurement combined with subsequent blink-based biomechanical measurements would allow estimating absolute IOP values over time.

Our approach has limitations. First, the variability of IOP elevation induced by the Valsalva maneuver presents challenges in achieving consistent IOP increments across trials. Additionally, IOP measurements during the Valsalva maneuver are taken before the acquisition of natural blinks, as it is not feasible to measure IOP using a portable tonometer and simultaneously record natural blinks during the application of the maneuver. This sequential process may introduce variability in the exact elevated IOP level during blink acquisition.

Furthermore, while our analysis focused on longitudinal corneal profile motion, it is known that the eye can retract during blinking[49–52] due to ELP and subsequently move forward upon eyelid release, contributing to the observed dynamics. Iskander et al.[53] have proposed three different models depicted in Fig. 6. Their results have shown that the longitudinal movement of the corneal profile during a blink is the superposition of eye movement and corneal deformation (Fig. 6c). Indeed, the inability to separate these effects in our current framework is another limitation. However, our results suggest that the Valsalva maneuver does not necessarily

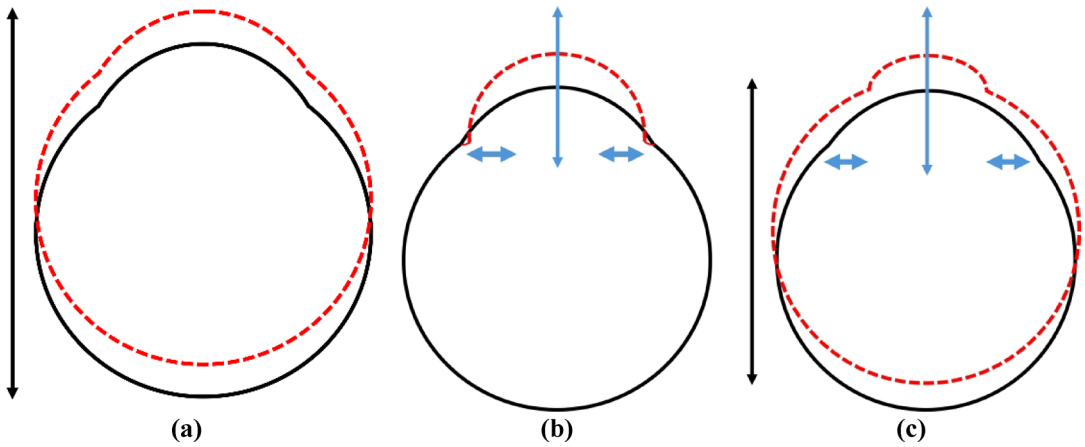

Fig. 6. Three models for the longitudinal corneal profile displacement during a blink. (**a**) Eye movement: the whole eye globe (black) moves forward to a new position (red dashed line), as indicated by the vertical arrow; (**b**) Cornea deformation: the red dashed profile represents the cornea deformed by eyelid pressure, with blue horizontal arrows indicating lateral compression and the blue vertical arrow showing the flattening direction; (**c**) Combined effect of eye movement (black arrow) and corneal deformation (blue arrows).

lead to greater globe movement. If it were true that this maneuver causes greater forward movement of the eye during the opening phase of a blink, one would expect A to consistently be higher than in the baseline IOP condition, with a statistically significant difference. The fact that a statistically significant difference is observed only for τ suggests that the Valsalva maneuver primarily results in a different rebound speed, which could be related to the IOP.

In addition to eye retraction, several studies have demonstrated that the globe undergoes small rotational movements during the blinking process, primarily during the lid closure phase, which contributes to the stabilization of visual perception[54]. Specifically, blinks are accompanied by downward and nasal rotations that precede lid closure, followed by an intorsional, upward return during reopening[50,55]. Kirchner et al.[56] further confirmed that these rotations typically range between 1–4° during natural blinks and represent a much smaller, subject-dependent component superimposed on the main translational motion of the globe. Therefore, since the analysis in the present study focused on the eye-opening phase, any residual rotation occurring during eyelid reopening is expected to be minimal and unlikely to significantly affect the longitudinal anterior segment dynamics quantified in our measurements. Finally, another concern is the potential influence of physiological changes unrelated to IOP during the Valsalva maneuver. While it is well-documented that the maneuver induces an increase in IOP, the exact mechanisms behind this increase remain unclear[57]. Therefore, the observed differences between the baseline IOP condition and the Valsalva condition may not be attributed only to an IOP increase but could also be influenced by other phenomena induced by the Valsalva maneuver, such as changes in ocular blood flow[22], venous pressure[58], or biomechanical properties of the anterior segment[59].

Future research should address key limitations. Specifically, separating the effects of corneal deformation and globe movement during blinking would allow direct analysis of corneal dynamics specifically induced by ELP. Moreover, a clinical study involving patients with glaucoma, both before and after administration of IOP-lowering medication, could validate the proposed method against applanation tonometry. This approach will overcome the limitations of the Valsalva maneuver and provide deeper insight into the relationship between corneal dynamics and IOP. Furthermore, this clinical study would integrate complementary ophthalmic measurements obtained from devices such as the Corvis ST and the Ocular Response Analyzer to provide a more complete characterization of the biomechanical properties of the cornea and to assess whether these parameters influence the IOP-dependent metrics derived from the blink-related anterior segment dynamics. Additionally, system illumination should be optimized to properly work under ambient lighting conditions typically found in a real-world scenario.

In conclusion, we have presented a novel, non-contact imaging system capable of tracking corneal profile motion during a natural, complete blink and analyzing blink-related anterior segment dynamics as an indicator of IOP variations. The proposed method does not directly measure IOP in mmHg but demonstrates the feasibility of blink-related anterior segment dynamics parameters as indirect markers of IOP changes. After appropriate miniaturization and calibration correlating these parameters with reference tonometric values, this approach may enable continuous, home-based assessment of IOP-dependent anterior segment dynamics, offering a realistic and accessible complementary tool for glaucoma management and early detection.

Data availability

The dataset used and analyzed in the current study is available from the corresponding author upon reasonable request.

Received: 9 September 2025; Accepted: 26 December 2025

Published online: 06 January 2026

References

1. Thylefors, B. & Négrel, A. D. The global impact of glaucoma. *Bull. World Health Organ.* **72**, 323–326 (1994).
2. Kang, J. M., Tanna, A. P. & Glaucoma *Med. Clin. North Am.* **105**, 493–510 (2021).
3. McMonnies, C. W. The clinical and experimental significance of blinking behavior. *J. Optometry*. **13**, 74–80 (2020).
4. Cruz, A. A. V., Garcia, D. M., Pinto, C. T. & Cechetti, S. P. Spontaneous eyeblink activity. *Ocul. Surf.* **9**, 29–41 (2011).
5. Kotecha, A., White, E., Schlottmann, P. G. & Garway-Heath, D. F. Intraocular pressure measurement precision with the Goldmann Applanation, dynamic Contour, and ocular response analyzer tonometers. *Ophthalmology* **117**, 730–737 (2010).
6. Chen, G. Z., Chan, I. S., Leung, L. K. K. & Lam, D. C. C. Soft wearable contact lens sensor for continuous intraocular pressure monitoring. *Med. Eng. Phys.* **36**, 1134–1139 (2014).
7. De Moraes, C. G., Jasien, J. V., Simon-Zoula, S., Liebmann, J. M. & Ritch, R. Visual field change and 24-Hour IOP-Related profile with a contact lens sensor in treated glaucoma patients. *Ophthalmology* **123**, 744–753 (2016).
8. Xu, J. et al. Highly transparent and sensitive graphene sensors for continuous and Non-invasive intraocular pressure monitoring. *ACS Appl. Mater. Interfaces*. **12**, 18375–18384 (2020).
9. Kim, K. H., Lee, J. O., Du, J., Sretavan, D. & Choo, H. Real-Time *In vivo* intraocular pressure monitoring using an optomechanical implant and an artificial neural network. *IEEE Sens. J.* **17**, 7394–7404 (2017).
10. Yang, C. et al. Wearable and implantable intraocular pressure biosensors: recent progress and future prospects. *Adv. Sci.* **8**, 2002971 (2021).
11. Raveendran, R. et al. Current innovations in intraocular pressure monitoring biosensors for diagnosis and treatment of Glaucoma—Novel strategies and future perspectives. *Biosensors* **13**, 663 (2023).
12. Shaw, A. J., Collins, M. J., Davis, B. A. & Carney, L. G. Eyelid pressure and contact with the ocular surface. *Invest. Ophthalmol. Vis. Sci.* **51**, 1911–1917 (2010).
13. Yoshioka, E. et al. Influence of eyelid pressure on fluorescein staining of ocular surface in dry eyes. *Am. J. Ophthalmol.* **160**, 685–692 (2015).
14. Feng, X., Li, J., Hua, Z. & Zhang, F. Low-light image enhancement based on multi-illumination Estimation. *Appl. Intell.* **51**, 5111–5131 (2021).
15. Di Nisio, A., D'Alessandro, V. I., Scarcelli, G., Lanzolla, A. M. L. & Attivissimo, F. Noise robustness evaluation of image processing algorithms for eye blinking detection. *Measurement* **239**, 115508 (2025).
16. Icare, I. C. Instruction Manual. (2023).
17. Nakakura, S. et al. Evaluation of rebound tonometer iCare IC200 as compared with IcarePRO and Goldmann applanation tonometer in patients with glaucoma. *Eye Vis.* **8**, 25 (2021).
18. Badakere, S. V. et al. Agreement of intraocular pressure measurement of Icare ic200 with Goldmann applanation tonometer in adult eyes with normal cornea. *Ophthalmol. Glaucoma*. **4**, 238–243 (2021).
19. Brody, S., Erb, C., Veit, R. & Rau, H. Intraocular pressure changes: the influence of psychological stress and the Valsalva maneuver. *Biol. Psychol.* **51**, 43–57 (1999).
20. Aykan, U., Erdurmus, M., Yilmaz, B. & Bilge, A. H. Intraocular pressure and ocular pulse amplitude variations during the Valsalva maneuver. *Graefes Arch. Clin. Exp. Ophthalmol.* **248**, 1183–1186 (2010).
21. Liu, W. C., Lee, S. M., Graham, A. D. & Lin, M. C. Effects of eye rubbing and breath holding on corneal Biomechanical properties and intraocular pressure. *Cornea* **30**, 855–860 (2011).
22. Sun, L. et al. Dual effect of the Valsalva maneuver on autonomic nervous system activity, intraocular pressure, schlemm's canal, and iridocorneal angle morphology. *BMC Ophthalmol.* **20**, 5 (2020).
23. Ronneberger, O., Fischer, P. & Brox, T. U-Net: convolutional networks for biomedical image segmentation. In *Medical Image Computing and Computer-Assisted Intervention – MICCAI 2015* Vol. 9351 (eds Navab, N. et al.) 234–241 (Springer International Publishing, 2015).
24. Mumuni, A. & Mumuni, F. Data augmentation: A comprehensive survey of modern approaches. *Array* **16**, 100258 (2022).
25. Badrinarayanan, V., Kendall, A., Cipolla, R. & SegNet: A deep convolutional Encoder-Decoder architecture for image segmentation. *IEEE Trans. Pattern Anal. Mach. Intell.* **39**, 2481–2495 (2017).
26. Sudre, C. H., Li, W., Vercauteren, T., Ourselin, S. & Jorge Cardoso, M. Generalised dice overlap as a deep learning loss function for highly unbalanced segmentations. In *Deep Learning in Medical Image Analysis and Multimodal Learning for Clinical Decision Support* Vol. 10553 (eds Cardoso, M. J. et al.) 240–248 (Springer International Publishing, 2017).
27. Taghanaki, S. A. et al. Combo loss: handling input and output imbalance in multi-organ segmentation. *Comput. Med. Imaging Graph.* **75**, 24–33 (2019).
28. Maczynska, E. et al. Air-Puff-Induced dynamics of ocular components measured with optical biometry. *Invest. Ophthalmol. Vis. Sci.* **60**, 1979 (2019).
29. Shaw, A. J., Collins, M. J., Davis, B. A. & Carney, L. G. Eyelid pressure and contact with the ocular surface. *Invest. Ophthalmol. Vis. Sci.* **51**, 1911 (2010).
30. Sakai, E., Shiraishi, A., Yamaguchi, M., Ohta, K. & Ohashi, Y. Blepharo-tensiometer: new eyelid pressure measurement system using tactile pressure sensor. *Eye Contact Lens*. **38**, 326–330 (2012).
31. Pult, H. et al. Spontaneous blinking from a tribological viewpoint. *Ocul. Surf.* **13**, 236–249 (2015).
32. Wang, J. et al. Assessment of eyelid pressure using a novel pressure measurement device in patients with Moderate-to-Severe dry eye disease. *Front. Med. (Lausanne)*. **9**, 833576 (2022).
33. Buehren, T., Collins, M. J. & Carney, L. Corneal aberrations and reading. *Optom. Vis. Sci.* **80**, 159–166 (2003).
34. Collins, M. J. et al. Factors influencing lid pressure on the cornea. *Eye Contact Lens*. **32**, 168–173 (2006).
35. Shaw, A. J., Collins, M. J., Davis, B. A. & Carney, L. G. Corneal refractive changes due to short-term eyelid pressure in downward gaze. *J. Cataract Refract. Surg.* **34**, 1546–1553 (2008).
36. Shaw, A. J., Collins, M. J., Davis, B. A. & Carney, L. G. Eyelid pressure: inferences from corneal topographic changes. *Cornea* **28**, 181–188 (2009).
37. Martínez-Abad, A. & Piñero, D. P. New perspectives on the detection and progression of keratoconus. *J. Cataract Refract. Surg.* **43**, 1213–1227 (2017).
38. Pniakowska, Z., Jurowski, P. & Wierzbowska, J. Clinical evaluation of corneal biomechanics following laser refractive surgery in myopic eyes: A review of the literature. *J. Clin. Med.* **12**, 243 (2022).
39. Lin, M. et al. Effects of eyelid pressure on corneal tomography and biomechanics: quantitative analysis using a novel blepharo-tensiometer. *Cont. Lens Anterior Eye*. **47**, 102313 (2024).
40. Barkana, Y. Clinical utility of intraocular pressure monitoring outside of normal office hours in patients with glaucoma. *Arch. Ophthalmol.* **124**, 793 (2006).
41. Sharts-Hopko, N. C. & Glynn-Milley, C. PRIMARY OPEN-ANGLE GLAUCOMA. *AJN Am. J. Nurs.* **109**, 40–47 (2009).
42. Leung, D. Y. L. & Tham, C. C. Normal-tension glaucoma: current concepts and approaches-A review. *Clin. Exper Ophthalmol.* **50**, 247–259 (2022).
43. Lee, B. L., Bathija, R. & Weinreb, R. N. The definition of normal-tension glaucoma. *J. Glaucoma*. **7**, 366–371 (1998).
44. Song, B. & Caprioli, J. New directions in the treatment of normal tension glaucoma. *Indian J. Ophthalmol.* **62**, 529 (2014).

45. Gramer, E. & Leydhecker, W. Glaukom Ohne Hochdruck. Eine klinische Studie*. *Klin. Monatsbl Augenheilkd.* **186**, 262–267 (1985).
46. Mallick, J., Devi, L., Malik, P. K. & Mallick, J. Update on normal tension glaucoma. *J. Ophthalmic Vis. Res.* **11**, 204–208 (2016).
47. Shields, M. B. Normal-tension glaucoma: is it different from primary open-angle glaucoma? *Curr. Opin. Ophthalmol.* **19**, 85–88 (2008).
48. Jonas, J. B. et al. Ocular hypertension: general characteristics and estimated cerebrospinal fluid pressure. The Beijing eye study 2011. *PLoS One.* **9**, e100533 (2014).
49. Evinger, C., Shaw, M. D., Peck, C. K., Manning, K. A. & Baker, R. Blinking and associated eye movements in humans, Guinea pigs, and rabbits. *J. Neurophysiol.* **52**, 323–339 (1984).
50. Bour, L. J., Aramideh, M. & De Ongerboer, B. W. Neurophysiological aspects of eye and eyelid movements during blinking in humans. *J. Neurophysiol.* **83**, 166–176 (2000).
51. Mas, D. et al. Noninvasive measurement of eye Retraction during blinking. *Opt. Lett.* **35**, 1884–1886 (2010).
52. Perez, J., Espinosa, J., Domenech, B., Mas, D. & Illueca, C. Blinking kinematics description through non-invasive measurement. *J. Mod. Opt.* **58**, 1857–1863 (2011).
53. Robert Iskander, D. & Kasprzak, H. T. Dynamics in longitudinal eye movements and corneal shape. *Ophthalmic Physiol. Opt.* **26**, 572–579 (2006).
54. Willett, S. M., Maenner, S. K. & Mayo, J. P. The perceptual consequences and neurophysiology of eye blinks. *Front. Syst. Neurosci.* **17**, 1242654 (2023).
55. Bergamin, O., Bizzarri, S. & Straumann, D. Ocular torsion during voluntary blinks in humans. *Invest. Ophthalmol. Vis. Sci.* **43**, 3438–3443 (2002).
56. Kirchner, J., Watson, T., Bauer, J. & Lappe, M. High-speed MRI recordings of eyeball lifting, Retraction and compression during blinks. *Preprint at.* https://doi.org/10.1101/2022.05.11.491482 (2022).
57. V, S., Bhansali, S., Kosti, R. & Balananda, P. L, N. Intraocular pressure changes during Valsalva maneuver. *Natl. J. Physiol. Pharm. Pharmacol.* **13**, 1887–1892 (2023).
58. Stodtmeister, R. et al. Retinal venous pressure is higher than the airway pressure and the intraocular pressure during the Valsalva manoeuvre. *Acta Ophthalmol.* **96**, e68–e73 (2018).
59. Kara, N. & Kenan, S. Effect of refractive status on Valsalva-induced anterior segment changes. *Int. Ophthalmol.* **38**, 1205–1210 (2018).

Acknowledgements

The authors thank Kevin Aroom, John Rzasa, and Martha Wang (Robert E. Fischell Institute for Biomedical Devices, University of Maryland) for their assistance in designing and developing the imaging system used in this study.

Author contributions

AI, GS conceived the project. AI, GS, VD planned experiments. VD performed experiments and data analysis. All authors discussed data. FA, ADN, AL, VD discussed and planned methods. VD wrote the manuscript. All authors revised the manuscript.

Funding

This study has been funded in part by TEDCO Maryland innovation initiative to AI and GS and the Medical device development fund to AI.

Declarations

Competing interests

The authors declare no competing interests.

Additional information

Correspondence and requests for materials should be addressed to G.S.

Reprints and permissions information is available at www.nature.com/reprints.

Publisher's note Springer Nature remains neutral with regard to jurisdictional claims in published maps and institutional affiliations.